CRYSTAL GROWTH & DESIGN

pubs.acs.org/crystal

Article

Dual Mode of Action of Organic Crystal Growth Inhibitors

Published as part of a Crystal Growth and Design virtual special issue in Celebration of the Career of Roger Davey

Rajshree Chakrabarti and Peter G. Vekilov*

Cite This: *Cryst. Growth Des.* 2021, 21, 7053−7064

Read Online

ACCESS | Metrics & More | Article Recommendations | Supporting Information

ABSTRACT: Crystallization often proceeds in media with rich chemical compositions. In pursuit of insight into how foreign compounds interact with the structures and dynamics that comprise crystal growth, we explore the mechanisms employed by protoporphyrin IX to inhibit the growth of etioporphyrin I crystals. Crystals of porphyrins exhibit potential for use as organic semiconductors, solar cells, and field-effect transistors. We employ solutions in 1-octanol and combine time-resolved *in-situ* atomic force microscopy (AFM) with scanning electron microscopy and absorption spectroscopy. We demonstrate that protoporphyrin IX does not sequester etioporphyrin I in soluble complexes, which would lower the amount of growth-competent etioporphyrin I. We show that the microscopic and mesoscopic structures on the crystal surface and their dynamics during growth unequivocally report on the interactions of the modifier with the crystal surface. AFM observations eliminate lattice strain caused by PPIX molecules, embedded in the top crystal layer or merely bound to it, as a factor for step inhibition. The lack of long-lasting strain allows steps to revert to uninhibited growth after the inhibitor is purged. We show that an inhibitor may bind to both kinks and crystal surfaces and thus exert a dual mode of suppression. We develop an analytical model for step growth in the presence of a dual-action modifier that highlights an antagonistic element of the cooperativity of the two modes of inhibition enforced by the decline of step edge free energy after the modifier associates to kinks. Our results demonstrate that dual-action inhibitors are superior regulators of crystal growth that afford the opportunity to fine-tune the degree of inhibition required to optimize the growth and shape of crystals of interest.

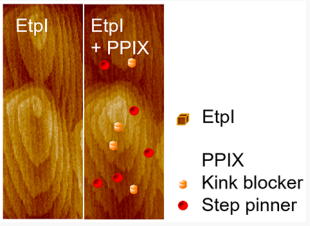

INTRODUCTION

Crystallization is an essential step in many biological, geological, and industrial processes.[1−10] Crystallization rarely occurs in environments that only include solute and solvent. The additional components of the crystallization medium may interact with both the solute and the crystal.[11] These interactions may accelerate or delay and even completely stunt growth.[12,13] Natural crystallization supplies numerous examples of how foreign compounds stimulate a variety of shapes, functionalities, and forms of the arising crystalline materials by modifying the rates of crystal nucleation and growth.[14] Ubiquitous strategies in industry rely on modifiers to control crystallization and empower efficient practices that elicit desired final product qualities.[15−19] Examples of crystallization that endangers human life and health include the formation of kidney stones,[20,21] heme detoxification in malaria parasites,[22,23] and cholesterol plaque formation,[24−26] and compounds found to suppress these instances of pathological crystallization have been promoted to drugs for the ensuing conditions.[27−35]

The classical crystal growth mechanisms assume that individual solute molecules attach to the edges of unfinished layers on the crystal surface, called steps.[36−41] Modifiers may sway any element of the crystal growth sequence. They may complex the solute and thus lower the concentration of growth-competent molecules and the crystallization driving force.[42] They may bind to the crystal surface[35] or inter in the top crystal layer;[43] both events may strain the crystal surface. The emergent strain elevates the chemical potential of the top crystal molecules, which brings it closer to the chemical potential of the solute and diminishes the crystallization driving force.

Even if a modifier adsorbed on the surface does not perturb the lattice sufficiently to raise the chemical potential of the surface molecules, it may still suppress step motion. A step growing around an adsorbed modifier is forced to bend, and the ensuing curvature, in accordance with the Gibbs−Thomson rule, lowers the force that drives step growth (Figure 1A);[22,33,34,44] this mechanism has been referred to as step pinning. Analytical and numerical models of this inhibition pathway,[23,44−53] concertedly with experiments,[54−57] predict potent step growth suppression up to complete growth cessation imposed by moderate inhibitor concentrations

Received: August 23, 2021
Revised: October 28, 2021
Published: November 18, 2021

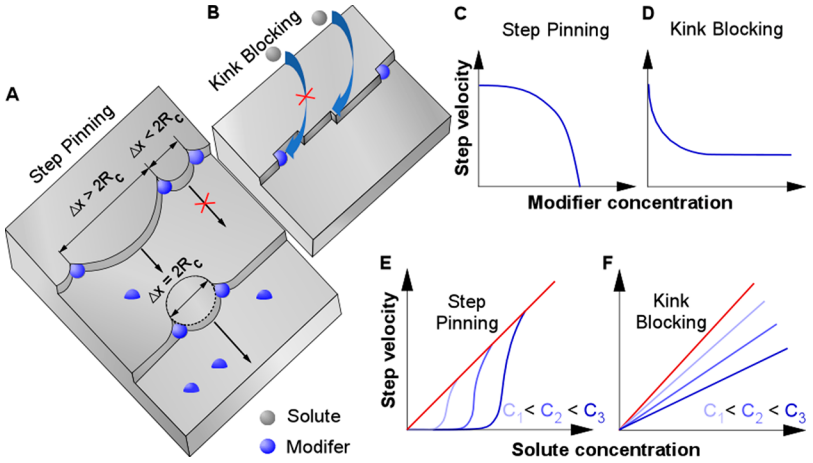

Figure 1. The classical mechanisms of step inhibition. (A, B) Schematic illustrations of step inhibition by step pinners and kink blockers. (A) Step pinners adsorb on the terraces between steps and force steps to bend to grow between two pinners. If the separation between two pinners Δx is shorter than the critical two-dimension diameter $2R_c$, step grows ceases. If Δx is longer but comparable to $2R_c$, step growth is delayed. (B) Kink blockers associate with the kinks and obstruct the access of solute molecules. (C–F) Schematic representations of the correlations between the step velocity with the concentration of the modifier, in (C, D), and the solute, in (E, F) in the cases step pinning, in (C, E), or kink blocking, in (D, F), derived from analytical models of the two inhibition modes. In (E, F), C_1, C_2, and C_3 indicate increasing modifier concentrations.

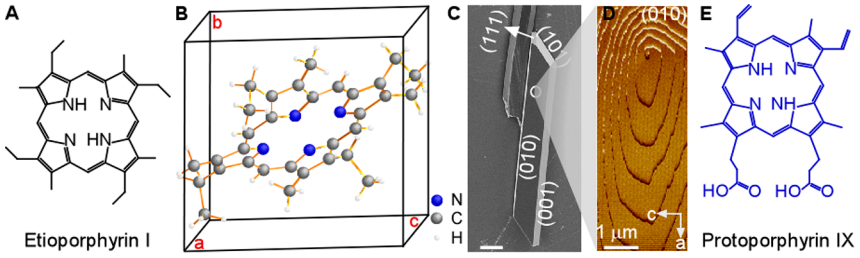

Figure 2. Etioporphyrin I molecule and crystals and protoporphyrin IX. (A) The structure of etioporphyrin I (EtpI). (B) The structure of EtpI crystals in *P*1 space group (Cambridge Structural Database REFCODE WOBVUF);[76] the symbols depicting N, C, and H are shown at the lower right. The lattice parameters are a = 6.88 Å, b = 9.91 Å, c = 10.35 Å, α = 88.47°, β = 79.70°, and γ = 77.44°. (C) Scanning electron micrograph of EtpI crystals grown in octanol; labels indicate the major crystal faces, identified by single crystal X-ray diffraction. (D) *In-situ* atomic force microscopy image of the (010) face of an EtpI crystal showing steps emerging from a screw dislocation outcropping on the face. (E) The structure of protoporphyrin IX (PPIX).

(Figure 1C). Higher solute concentrations push down the critical two-dimensional radius and allow steps to penetrate the modifier fence, invoking a S-shaped correlation between step growth rate and crystallization driving force (Figure 1E).[52,53,55,58,59]

Alternatively, modifiers may attach to the growth sites, the kinks, and block access of solute molecules *en route* to incorporate into the crystal (Figure 1B);[33,40] this modifier activity is sometimes called kink blocking. Owing to the dynamics at the step edge, where kinks are continuously generated, kink blocking does not enforce complete growth cessation even at high inhibitor concentrations (Figure 1D),[23] and the correlation between the step velocity and the solute concentration remains linear (Figure 1F).[23,40] The former two modes of modifier action, solute complexation and surface strain, have been classified as thermodynamic, whereas step pinning and kink blocking have been designated, somewhat arbitrarily, as kinetic.[19,32,35]

The recent interest in crystallization in complex natural and engineered systems has exposed a plethora of nonclassical behaviors.[60–63] The most common pathway veering outside the classical ruts is crystal growth by incorporation of preformed oligomers[61,64] or liquid, amorphous, and crystalline mesoscopic solute assemblies.[2,63,65–68] Nonclassical crystallization opens new targets for crystallization modifiers. Modifiers may both suppress and enhance the formation of precursors and modulate their properties as a means to accelerate or inhibit crystal growth.[19,69–71]

An emerging exploration topic is the cooperatively between two modifiers, which, if applied individually, adopt distinct inhibition mechanisms.[6,23,72–75] A variant of the question of modifier cooperativity is how a growing crystal responds to a single modifier that simultaneously employs two modes of crystallization inhibition.[47] To address this latter question, we enlist as a model the growth of etioporphyrin I (EtpI) crystals. EtpI (Figure 2A–D) represents a class of crystals that carry promising optical and electronic properties for use as semiconductors, solar cells, and field-effect transistors.[76–78] We monitor the response of the growth of EtpI crystals to protoporphyrin IX (PPIX), a free base porphyrin, whose structure differs from that of EtpI by the presence of two propionic and two vinyl groups (Figure 2E). The similarity of the structure of the additive to that of the solute extends a bridge to previous studies on how tailor-made auxiliaries and molecular imposters affect the growth of organic crystals.[79–81] We dissolve EtpI and PPIX in 1-octanol.[82]

https://doi.org/10.1021/acs.cgd.1c00971
Cryst. Growth Des. 2021, 21, 7053–7064

RESULTS AND DISCUSSION

Effects of Protoporphyrin IX on the Size and Shape of EtpI Crystals. A crystal's size and shape are among the central determinants of its utility.[41,83] EtpI crystals terminate with {010}, {001}, {101}, and {111} faces.[76,82] The {010} faces are the largest, and the crystals preferentially position on a substrate with a (010) face upward. With this orientation, the crystal length l increases owing to growth in the ⟨101⟩ and ⟨111⟩ directions (Figure 3A), whereas growth in the ⟨001⟩ directions contributes to the crystal width w (Figure 3A). To assess how PPIX modifies the EtpI crystal shape, we grew EtpI crystals in the presence of PPIX concentrations that varied from 0 to 20 μM and imaged by scanning electron microscopy (SEM) the populations of crystals grown for 7 days (Figure 3D–I). All growth runs were carried out in triplicate, and l and w of at least 30 crystals were measured at each PPIX concentration. As PPIX concentrations increase, both the average crystal length and width monotonically shorten; at 15 μM PPIX, l is shorter by about 60% and w by about 40% than those of the control (Figure 3B,C). At its highest concentration, 20 μM, PPIX caused crystal twinning and intergrowth (Figure 3I), which hampered accurate length and width measurements. The shorter length of the crystals grown in the presence of PPIX manifests strong inhibition of the growth of the {101} and {111} faces of EtpI crystals by PPIX (Figure 3J,K), whereas the shorter width implies that PPIX similarly inhibits the growth of the {001} faces.

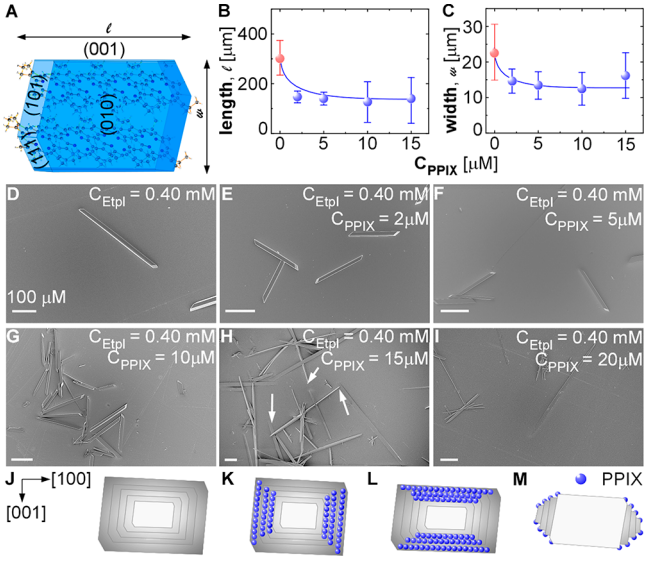

Figure 3. The response of EtpI crystal size and morphology to PPIX. (A) The habit of EtpI crystals calculated using Mercury[84] with parameters obtained from CSD entry REFCODE WOBVUF[76] showing the dominant faces and the definitions of the crystal length l and width w. (B, C) Variations of the average length l, in (B), and width w, in (C), of EtpI crystals grown for 7 days at 25 °C in 0.40 mM solutions in octanol in the presence of increasing PPIX amounts. Error bars denote the standard deviation from the average of at least 30 independent measurements. (D–I) Representative scanning electron micrographs of etioporphyrin I crystals grown in the absence, in (D), and in the presence of the protoporphyrin IX concentrations listed in each panel. Arrows in (H) point to tapered crystal apexes. (J–L) Schematic illustrations of the shortening of l, in (K), and of w, in (L), compared to the uninhibited crystal shape, in (J), due to growth inhibition by PPIX, represented as blue spheres. (M) Schematic illustration of crystal tapering due to enhanced adsorption of PPIX molecules near the crystal edges.

At 15 μM, PPIX crystals grew narrower close to their apexes than at their respective axial midpoints (Figure 3H). Such tapered shapes have been attributed to blocking of steps on the orthogonal faces as they approach a shared edge, induced by enhanced supply of inhibitors to the edge (Figure 3M).[85] The symmetric tapering at opposite apexes (Figure 3H) indicates that PPIX interactions with the (101) face are equal to those with the $(\bar{1}0\bar{1})$ face, and the PPIX interactions with the (111) face match those with the $(\bar{1}\bar{1}\bar{1})$ face.

Lack of Complexation between Etioporphyrin I and Protoporphyrin IX. A plausible scenario to explain the uniform suppression of growth of the {111}, {101}, and {001} faces by PPIX assumes sequestration of EtpI in soluble complexes with PPIX, which lowers the amount of EtpI available for crystal growth and the crystallization driving force. Complexation could potentially completely stunt the growth of EtpI crystals if the residual concentration of unliganded EtpI drops to values at or below its solubility C_e.

To test whether complexation represents the prevalent mode of inhibition of EtpI crystal growth by PPIX, we characterized the EtpI–PPIX binding equilibria in octanol, using a method based on absorption spectroscopy, previously used to test the binding of hematin to antimalarial drugs.[33] The individual absorption spectra of EtpI and PPIX both reveal distinct Q bands (Figure 4A), commonly attributed to two purely electronic transitions (0–0) and two mixed vibronic transitions (0–1) of the porphyrin ring.[86−90] The individual spectra recorded at several concentrations of each compound supplied their respective extinction coefficients in the examined wavelength range. The concentrations of PPIX were 2–40-fold lower than those of EtpI to match the concentration ratios tested in the crystal growth experiments (Figure 4A). As a result of this compositional asymmetry, the intensity contributed by PPIX to the absorption peaks of the mixtures is lower than that of EtpI. The PPIX contributions present as well-detectable shoulders on the right side of the EtpI peaks around 570 and 620 nm, as a weaker shoulder of the EtpI peak at around 520 nm and a shape change of the EtpI peak at around 490 nm (Figure 4A). Importantly, no new peaks that may belong to a potential EtpI–PPIX complex and no isosbestic points[33] arise in the spectra of the mixtures (Figure

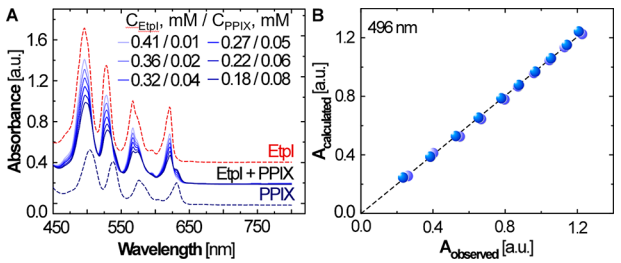

Figure 4. Characterization of mixed EtpI and PPIX solutions by absorption spectroscopy. (A) Individual spectra of EtpI and PPIX dissolved in octanol (dashed lines) and spectra of six EtpI–PPIX mixed solutions of distinct compositions. (B) The absorbances at 496 nm of 10 mixed solutions of EtpI and PPIX with distinct concentrations equal the absorbances calculated assuming no complexation between EtpI and PPIX. Two independent tests are shown. The dashed straight line represents the best linear regression fit to the two data sets and has a slope of 1.0 and intercept of 0.0.

https://doi.org/10.1021/acs.cgd.1c00971
Cryst. Growth Des. 2021, 21, 7053−7064

4A). Furthermore, the spectra of the six mixed solutions of EtpI and PPIX at distinct concentration ratios equaled the sums of the spectra of the individual components weighted with their respective concentrations (Figure 4A).

As a second test, we measured the absorbances at 496 nm of 10 mixed EtpI−PPIX solutions (Table S1), which again proved equal to the calculated sums of the individual absorbances of EtpI and PPIX (Figure 4B). The congruity of the measured and calculated spectra and absorbances of mixtures of EtpI and PPIX deny the existence of an EtpI−PPIX complex, which would exhibit a unique absorbance spectrum and lower the concentrations and absorbances of the two porphyrins. The spectroscopic characterization of mixed EtpI−PPIX solutions demonstrates that complexation between the two porphyrins is minimal and certainly insufficient to lower the concentration of EtpI to the extent necessary for the recorded inhibition of EtpI crystal growth.

The Molecular Mechanism of PPIX Action. The lack of complexation between EtpI and PPIX advocates that PPIX suppresses the growth of EtpI crystal faces by interacting with the crystal surfaces. To glean molecular-level details on how PPIX impacts the structures and dynamics of EtpI crystal surfaces, we monitored the basal (010) face with atomic force microscopy (AFM) *in situ* during growth from solutions in octanol. The microscopic and mesoscopic structures on the crystal surface and their dynamics during growth sensitively discriminate three possible interactions of the modifier with the crystal surface: induction of lattice strain, step pinning, or kink blocking.

The crystal surface structure in solutions of EtpI alone constitutes the baseline to assess the inhibitor activity. The EtpI crystals select a classical mechanism of growth. The (010) face structures as unfinished crystal layers wound into spirals emanating from screw dislocations that outcrop on that face (Figure 5A). Solute molecules associate with the edges of the unfinished layers, the steps, and they grow, and the spiral continuously turns as new layers emerge at its center. As the steps move away from the dislocation outcrop, the anisotropy of step growth sculpts the shape of the dislocation hillock.[54,91,92] The lack of inversion centers, mirror planes, or two-fold axes in the P1 EtpI crystal symmetry group disconnects step growth in the [100], or $\vec{a}$, direction from that in the opposite [$\bar{1}$00] direction and in the [001], or $\vec{c}$, direction from growth in the [00$\bar{1}$] direction (Figure 5A). Steps growing fast in the [100] direction reach farthest from the dislocation outcrop, whereas steps growing in the [$\bar{1}$00] direction are the slowest. The intermediate velocities of steps growing in the [001] and [00$\bar{1}$] directions dictate the lanceolate shape of the step spiral (Figure 5A). Importantly, this shape persists at varying EtpI concentrations and argues that the anisotropy of step growth is independent of the solute concentration.

AFM observations eliminate lattice strain, caused by PPIX molecules embedded in the top crystal layer or merely bound to it. Both mechanisms require a strictly defined combination of the chemical potentials of the modifier and the solute that constrains the activity of this inhibition modes to select locations on the crystal surface and to limited time spans.[35] In contrast to these expectations, the impact of PPIX on the step pattern on the (010) face is uniform (Figure 5B), and the step pattern remains largely similar to that in solutions without PPIX (Figure 5A).

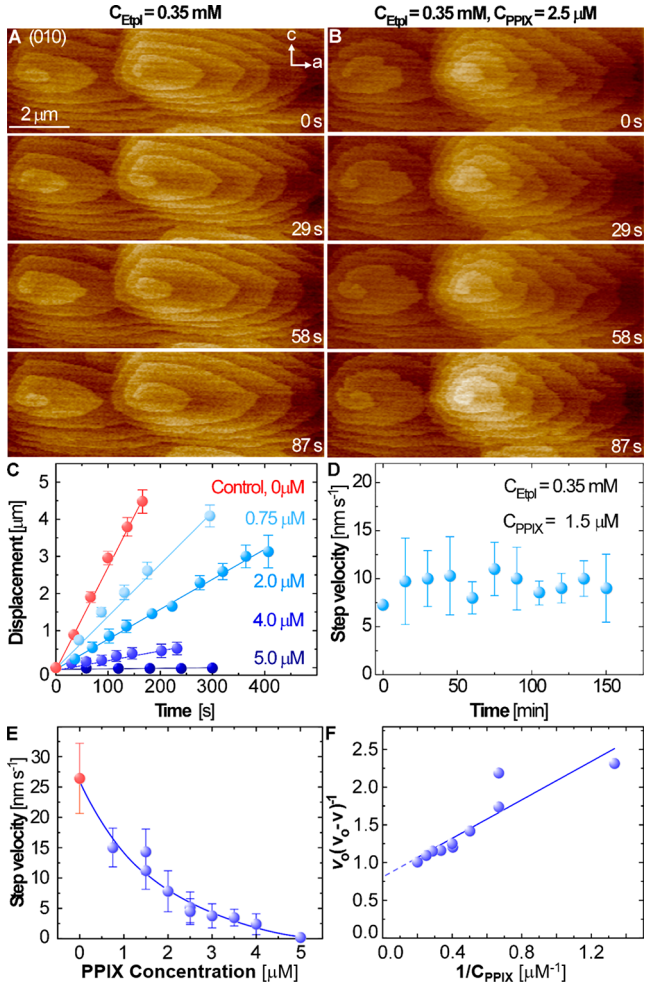

Figure 5. Growth of EtpI steps in the presence of PPIX. (A, B) Time-resolved situ atomic force microscopy images of the evolution of the growth spiral on a (010) face of EtpI crystals growing in a 0.35 mM solution in octanol in (A) and in the presence of 2.5 μM PPIX in (B, C). Evolutions of step displacements in the [100], or $\vec{a}$, direction in solutions of EtpI at concentration 0.35 mM, in red, and in the presence of listed amounts of PPIX, in blue. Error bars represent the standard deviations from the respective averages over about 30 measurements for each time. Straight lines represent best linear regression fits to the data. (D) The evolution of the step velocity in the [100] direction in a solution of 0.35 mM EtpI in the presence of 1.5 μM PPIX. (E) The correlation of the step velocity in the [100] direction and the C_{PPIX} in 0.35 mM EtpI solutions. The line is just a guide for the eye. In (D, E), error bars represent the standard deviations of the slopes of the displacement−time correlations, as in (C). (F) The correlation of the step velocity with C_{PPIX} in reciprocal coordinates. The solid straight line represents best linear regression fit to the data. The deviating point at C_{PPIX}^{-1} = 0.7 mM^{-1} was excluded from the analysis. Dashed line extension of the straight line highlights the intercept of the correlation.

The distances away from the dislocation outcrop that a step reaches increase proportionally to the elapsed time both in pure EtpI solutions and in the presence of as much as 5 μM PPIX (Figure 5C). The slopes of the step displacement−time correlations define the step velocity v. The quantity v presents a sensitive indicator of the kinetics of incorporation of molecules into the kinks and the concurrent processes which engage PPIX. A potential interment of PPIX molecules into the top crystal layer would elicit lattice strain, which would depress

https://doi.org/10.1021/acs.cgd.1c00971
Cryst. Growth Des. 2021, 21, 7053−7064

the force driving further PPIX incorporation. The resulting slow accumulation of the PPIX molecule embedded in the crystal surface would continuously escalate the retardation of step motion due to lattice stress, and we would expect to see a continuously diminishing v. In contrast to these expectations, v is steady in time for up to 150 min (Figure 5D) which indicates, concurrently with the uniform response of the surface morphology to PPIX, that lattice strain is not a part of the mechanism employed by PPIX to suppress EtpI crystal growth.

The step velocity of etioporphyrin I at a constant solute concentration rapidly decays as C_{PPIX} increases (Figure 5E). This immediate step growth suppression conforms to expectations for PPIX blocking the kinks (Figure 1B,D) and is in contrast to the predictions of the step pinning model of step inhibition (Figure 1A,C). To further illuminate the activity of PPIX, we derive an expression for the correlation between C_{PPIX} and v assuming that the activity of PPIX is restricted to association to kinks. We rely on a fundamental tenet of crystallization that v is proportional to the kink density n_k.[36,38,39,93,94] We designate the fraction of kinks occupied by inhibitor molecules θ_k. This θ_k may be limited by kink generation that occurs on time scales comparable to those of inhibitor adsorption.[23] We account for this limitation by a multiplier ξ, $0 \le \xi \le 1$. With these assumptions

$$v \propto n_k = n_{k,0}(1 - \xi\theta_k) \text{ and } v = v_0(1 - \xi\theta_k) \quad (1)$$

where v_0 and $n_{k,0}$ are the values of v and n_k in the absence of inhibitors and n_k is the density of kinks unoccupied by PPIX. As $\theta_k \to 1$ v asymptotically reaches its low threshold

$$v_{sat} = v_0(1 - \xi) \text{ and } v_0\xi = v_0 - v_{sat} \quad (2)$$

Combining eqs 1 and 2,

$$v = v_0 - (v_0 - v_{sat})\theta_k \quad (3)$$

We model θ_k with the Langmuir adsorption isotherm, which assumes a finite number of equivalent adsorption sites, no interactions between adsorbed molecules, a desorption rate independent of the solution concentration of the inhibitor, and equilibrium between inhibitors on the surface and in the bulk. Under these assumptions

$$\theta_k = \frac{K_{Lk}C_{PPIX}}{1 + K_{Lk}C_{PPIX}} \quad (4)$$

where K_{Lk} is the Langmuir constant for adsorption of PPIX to kinks, and we obtain

$$v = v_0\left(1 - \xi\frac{K_{Lk}C_{PPIX}}{1 + K_{Lk}C_{PPIX}}\right) \quad (5)$$

Equation 5 reveals that the functional relation between v and the solute concentration does not modify in response to the activity of a kink blocker, and only the coefficient of proportionality reduces by a factor dependent on C_{PPIX}. Furthermore, eq 5 predicts that as C_{PPIX} increases, v decreases monotonically from v_0 at $C_{PPIX} = 0$ to its saturation value v_{sat} defined in eq 2. These two signature behaviors of kink blockers are reflected in the respective schematic plots (Figure 1D,F).

The relationship in eq 5 linearizes in coordinates v_0 $(v_0 - v)^{-1}$ as a function of C_{PPIX}^{-1},

$$v_0 - v = (v_0 - v_{sat})\frac{K_{Lk}C_{PPIX}}{1 + K_{Lk}C_{PPIX}} \quad (6)$$

$$\frac{v_0}{v_0 - v} = \frac{v_0}{v_0 - v_{sat}} + \frac{v_0}{v_0 - v_{sat}}\frac{1}{K_{LK}C_{PPIX}} \quad (7)$$

The correlation v_0 $(v_0 - v)^{-1}(C_{PPIX}^{-1})$ employing the $v(C_{PPIX})$ data is indeed reasonably linear (Figure 5F) and affirms that PPIX suppresses EtpI crystal growth by blocking the kinks along the steps. Closer inspection, however, informs that the intercept of this correlation, which, according to eq 2, defines $\xi^{-1} = v_0/(v_0 - v_{sat})$, is smaller than unity, implying that v_{sat} is negative, an unphysical conjecture. The conflict with the assumption of the straightforward kink blocking model also manifests in the $v(C_{PPIX})$ correlation (Figure 5E), in which v reaches zero (Figure S1) while still dependent on C_{PPIX}, in contradistinction from the asymptotic independence of v of C_{PPIX} as v_{sat} approaches, predicted by eq 5 and illustrated in Figure 1D.

To elucidate the mystery posed by the $v(C_{PPIX})$ data at constant C_{EtpI}, we recruit the other behavior, which distinguishes the two kinetic mechanisms of step inhibition, kink blocking, and step pinning, the $v(C_{EtpI})$ correlation at constant C_{PPIX}. If PPIX activity is indeed limited to blocking kinks, we expect $v(C_{EtpI})$ to mimic the correlation in the absence of PPIX with a lower scaling factor. Were PPIX to adsorb on the terraces between steps and force the steps to bend as they squeeze between the stoppers in their way, we expect a complex $v(C_{EtpI})$ that divides into three segments. At low C_{EtpI}, the low thermodynamic driving force for crystallization $\Delta\mu = k_BT\ln(C_{EtpI}/C_e)$ (k_B, Boltzmann constant; T, temperature; C_e, EtpI solubility) would authorize a large radius of the two-dimensional critical nucleus $R_c = \Omega\gamma/\Delta\mu$. Here Ω is the volume occupied by one EtpI molecule in the crystal—in the P1 space group, Ω equals the unit cell volume—and γ is the surface free energy of the step edge. If R_c is greater than the mean spacing between pinners adsorbed on the crystal surface, the step growth stalls even though the C_{EtpI} is above the solubility. This C_{EtpI} range is called "dead zone". At a slightly higher C_{EtpI}, at which R_c is smaller but comparable to the mean spacing between pinners, v vigorously accelerates as higher C_{EtpI} drives R_c to way smaller than the pinner spacing. At C_{EtpI} two- or three-fold greater than the dead zone width, R_c is sufficiently small that the steps are no longer sensitive to the pinners, and v attains its dependence on solute concentration as in a pure solution (Figure 1E). The second segment, where v sharply responds to greater C_{EtpI}, shifts to higher C_{EtpI} at higher modifier concentrations (Figure 1E).[52,53,55]

The AFM-measured correlation between the step velocity v and C_{EtpI} at constant $C_{PPIX} = 1.5$ μM exhibits behaviors typical for both steps pinning and kink blocking (Figure 6A). Similar to expectations for step pinning, this correlation divides into three segments: a dead zone for $C_{EtpI} - C_e \le 0.13$ mM, swift acceleration of v for 0.13 μM $< C_{EtpI} - C_e \le 0.19$ M, and proportionality between v and C_{EtpI} for $C_{EtpI} - C_e > 0.19$ mM (Figure 6A). The slope of the linear correlation in the latter segment, however, is about two-fold lower than that in solution without PPIX (Figure 6A), indicating that PPIX also blocks the kinks and obstructs the association of EtpI molecules to them. To better understand the dual action of PPIX on EtpI steps, we develop an analytical model of combined step pining and kink blocking and compare its predictions to the $v(C_{EtpI}, C_{PPIX})$ correlations measured with AFM.

https://doi.org/10.1021/acs.cgd.1c00971
Cryst. Growth Des. 2021, 21, 7053−7064

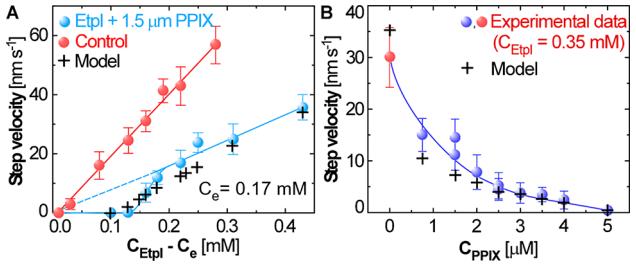

Figure 6. The correlations between the step velocity v and the concentrations of EtpI C_{EtpI} and PPIX C_{PPIX} in solutions of both porphyrins. (A) The $v(C_{EtpI})$ correlation in solution of EtpI only (red spheres) and in the presence of 1.5 μM PPIX (blue spheres). Error bars represent the standard deviations of the slopes of the respective displacement−time correlations. Solid straight lines represent best linear regression fits to the data. Blue dashed line extends the linear $v(C_{EtpI})$ segment at 1.5 μM PPIX to $C_{EtpI} - C_e = 0$. The prediction of the model of PPIX activity by combined kink blocking and step pinning (crosses). (B) Juxtaposition of the $v(C_{PPIX})$ correlation at C_{EtpI} = 0.35 mM and $C_{EtpI} - C_e$ = 0.18 mM (blue spheres) with the model prediction (crosses). The line through the measured velocities is just a guide for the eye.

Analytical Model of the Dual Action of PPIX. We consider the motion of steps governed by three phenomena: (1) Modifier molecules adsorb on the terraces and enforce step curvature, which elevates the chemical potential of the curved steps and constricts the driving force for step growth.[95] (2) Modifiers associate with the kinks and bar incorporation of solute molecules to some of the kinks. (3) Importantly, conforming to the Gibbs rule of adsorption, a corollary of the second law of thermodynamics, association of modifiers with the kinks is only possible if they reduce the surface free energy γ of the step edge. The decrease of γ regulates how the steps respond to greater curvature.

The supersaturation $\Delta\mu = k_BT \ln(C_{EtpI}/C_e)$, where $\Delta\mu = \mu - \mu_e = \mu - \mu_c$, and μ, μ_e, and μ_c are the chemical potentials of the solute in the solution, in a solution at equilibrium with the crystal, and in the crystal, respectively; C_{EtpI} is the solute concentration; and C_e is the EtpI solubility. This definition relies on the assumption that the ratio of solute activity coefficients in the supersaturated solution and at equilibrium is close to 1. For brevity, we introduce σ, defined as $\sigma \equiv \Delta\mu/k_BT = \ln(c_{EtpI}/C_e)$. According to the transition state theory, the rate of a reversible chemical reaction is proportional to $\left(\exp\frac{\Delta\mu}{k_BT} - 1\right)\beta$.[96] Accounting for the molecular size, the kink density, the activation barrier for incorporation, factors included in the step kinetic coeeficint β, and the change in molecular density upon crystallization via the product ΩC_e, the step velocity relates to the supersaturation as[39,40]

$$v = \beta\Omega C_e\left(\exp\frac{\Delta\mu}{k_BT} - 1\right) = \beta\Omega(C_{EtpI} - C_e) \tag{8}$$

The predicted linear $v(C)$ correlations have been recorded for numerous crystals growing in supersaturated solutions of solute only[97] and is obeyed by EtpI crystallization (Figure 6A).

We assume the modifier molecules adsorb on the crystal surface with molecular surface concentration $n_S = \theta_S/S_0$, where θ_S is the surface coverage and S_0 is the area of one adsorption site. For inhibitors, whose molecular size is commensurate with that of the solute, S_0 is the dot product of the two lattice vectors parallel to the upward facing crystal face. We evaluate the average distance between stoppers as

$$L = n_S^{-0.5} = \sqrt{S_0/\theta_S} \tag{9}$$

To evaluate θ_S, we assume that adsorption on the crystal surface, similar to adsorption at the kinks, follows the Langmuir relation between θ_S and the solution concentration C_{PPIX},

$$\theta_P = K_{LS}C_{PPIX}/(1 + K_{LS}C_{PPIX}) \tag{10}$$

where K_{LS} is the respective Langmuir constant, distinct from K_{Lk}, the Langmuir constant for adsorption at the kinks. We assume that pinners separated by distance L enforce step curvature with radius $R = L/2$. We obtain

$$R = \frac{1}{2}\sqrt{S_0\frac{1 + K_{LS}C_{PPIX}}{K_{LS}C_{PPIX}}} \tag{11}$$

According to the Gibbs−Thomson relation, a step with a radius of curvature R is in equilibrium with a solution of concentration C_{eR}, which is greater than the equilibrium concentration of a straight step C_e by

$$\ln\left(\frac{C_{eR}}{C_e}\right) = \frac{\Omega\gamma}{Rk_BT} \tag{12}$$

where γ is the surface free energy of the step edge. Equation 12 inverts the familiar application of the Gibbs−Thomson relation to define the radius R_c of a two-dimensional island in equilibrium with a solution with a concentration C_{EtpI} greater than the solubility C_e

$$R_c = \frac{\Omega\gamma}{k_BT\ln(C_{EtpI}/C_e)} \tag{13}$$

Unifying eqs 11 and 12, we obtain an expression for the critical supersaturation σ_d, below which a step cannot penetrate the inhibitor fence and growth ceases

$$\sigma_d = \ln\left(\frac{C_{eR}}{C_e}\right) = \frac{2\Omega\gamma}{k_BT}\sqrt{\frac{1}{S_0}\frac{K_{LSP}C_{PPIX}}{1 + K_{LS}C_{PPIX}}} \tag{14}$$

Equation 14 defines the dead zone width. This expression for σ_d is identical to the one derived by Weaver and De Yoreo.[49,50]

From eq 12, the solution concentration at equilibrium of a curved step with radius R is

$$C_{eR} = C_e \exp\frac{\Omega\gamma}{Rk_BT} \tag{15}$$

At a concentration $C_{EtpI} > C_{eR}$, a step with radius of curvature R grows with velocity

$$v_R = \beta\Omega(C_{EtpI} - C_{eR}) = \beta\Omega\left(C_{EtpI} - C_e\exp\frac{\Omega\gamma}{Rk_BT}\right)$$
$$= v_\infty\frac{C_{EtpI} - C_e\exp\frac{\Omega\gamma}{Rk_BT}}{C_{EtpI} - C_e} \tag{16}$$

where v_∞ is the velocity of a straight step, defined in eq 8. An equivalent form of this relation is[49]

$$v_R = v_\infty\left(1 - \frac{e^{\sigma_d} - 1}{e^{\sigma} - 1}\right) \tag{17}$$

https://doi.org/10.1021/acs.cgd.1c00971
Cryst. Growth Des. 2021, 21, 7053−7064

Combining eq 16 with eq 11 on the relation between the step radius of curvature R, dictated by the surface concentration of step pinners, and the bulk concentration of step pinners C_{PPIX} engenders a relation between the v_R and C_{PPIX}

$$v_R = \frac{v_\infty}{C_{EtpI} - C_e}\left(C_{EtpI} - C_e \exp\frac{2\Omega\gamma}{k_BT}\sqrt{\frac{K_{LS}C_{PPIX}}{S_0(1 + K_{LS}C_{PPIX})}}\right) \quad (18)$$

According to eq 18, at constant C_{EtpI} the velocity v_R of a step enforced by step pinners with solution concentration C_{PPIX} decreases monotonically from v_∞ at $C_{PPIX} = 0$, at which the step curvature $R = \infty$, to zero as C_{PPIX} reaches the limit defined by eq 14 with $C_{eR} = C_{EtpI}$ (Figure 1C). At low C_{PPIX}, the decline of v_R is gentle, but intensifies exponentially as C_{PPIX} moderately increases (Figure 1C). At constant C_{PPIX}, v_R is held at zero as long as C_{EtpI} stays lower than C_{eR} defined by eq 14. At $C_{EtpI} > C_{eR}$, eq 18 predicts a linear increase of v_R following a trend that lies parallel to that in a pure solution but lower due to the exaggerated value of C_{eR}. The linear $v_R(C_{EptI})$ correlation predicted by eq 18 stands in contrast to S-shaped dependences (Figure 1E) observed in experiments and attributed to step pinning.[55,98]

Notably, experiments measure not v_R, but a step velocity averaged over both curved and straight step segments that propagate between the lines of stoppers. Recent kinetic Monte Carlo results reveal that the surface distribution of step pinners has no effect on the average step velocity, i.e., steps with varying curvatures due to uneven distribution of pinner advance, on the average, as fast as steps with constant curvature imposed by uniformly distributed pinners of the same surface density.[51] Assessing the relative contributions to the measured averages of curved and straight step segments, however, has faced challenges. The original model of step pinning, by Cabrera and Vermilyea,[44] evaluated the effective step velocity as the geometric mean of the maximum velocity, corresponding to uninhibited step propagation in the gaps between the pinners and following the kinetic law in eq 8, and the minimum v due to pinning according to eq 18. In the step motion law, this mode of averaging invoked an exponent of 1/2 on the expression in parentheses in eq 18. Subsequent models assumed that the measured step velocity corresponds to an arithmetic mean[99] or just to the minimum velocity expressed by eq 18.[48] Additional factors—kink blocking by the pinners, step anisotropy, variable step curvature,[46] stopper mobility, slow stopper adsorption, and others—failed to predict quantitatively experimentally measured correlations between the step velocity and the solute concentration.[100] We surmise that this discrepancy between experiment and models emanates from the shared theoretical assumption that the relative contributions of straight and curved step segments are independent of the supersaturation. In fact, at high supersaturations, where $2R_c$ is substantially shorter than the mean separation between pinners, straight segments would dominate the statistics of step velocities, and the measured v would be close to that in solutions without and inhibitor. Accounting for supersaturation-dependent relative contributions of straight and curved steps to the effective step velocity controlled by step pinners is a worthy future task.

Considering the added activity of PPIX as a kink blocker, we evaluate how much the surface free energy γ of the step edge declines owing to adsorption of PPIX to the kinks. We assume that $n_{k,b} = n_{k,0} - n_k$, the density of kinks occupied by adsorbed PPIX, is equal to the number of PPIX molecules adsorbed at the kinks. With this assumption, $n_{k,b}$ complies with the Gibbs equation of adsorption[95]

$$\frac{n_{k,b}}{a} = -\frac{d\gamma}{d\mu_{PPIX}} \quad (19)$$

where a is the step height and μ_{PPIX} is the chemical potential of PPIX in the solution. Owing to the low inhibitor concentrations, the interactions between inhibitor molecules are weak and $\mu_{PPIX} = \mu_{PPIX,0} + k_BT \ln C_{PPIX}$, where $\mu_{PPIX,0}$ is the standard value of μ_{PPIX}. The sum of occupied and free kinks $n_k + n_{k,b} = n_{k,0}$ and $n_{k,b} = \theta_k\xi n_{k,0}$.

We integrate the Gibbs equation and substitute the relations for $n_{k,b}$ and μ_{PPIX} to obtain

$$-\Delta\gamma = \int_0^{C_{PPIX}} \frac{n_{k,b}}{a} d\mu_{PPIX} = \int_0^{C_{PPIX}} \frac{\theta_k\xi n_{k,0}}{a} k_BT d\ln C_{PPIX} = \int_0^{C_{PPIX}} \frac{K_{Lk}}{1 + K_{Lk}C_{PPIX}} \frac{n_{k,0}\xi}{a} k_BT dC_{PPIX} \quad (20)$$

and

$$-\Delta\gamma = \frac{k_BT\xi n_{k,0}}{a}\int_0^{C_{PPIX}} \frac{K_{Lk}dC_{PPIX}}{1 + K_{Lk}C_{PPIX}} dC_{PPIX} = \frac{k_BTn_{k,0}}{a}\xi \ln(1 + K_{Lk}C_{PPIX}) \quad (21)$$

Equation 21 is equivalent to the venerable Szyszkowski empirical relation.[101]

Incorporating eqs 5 and 21 into eq 18 begets

$$v_R = \beta\Omega\left(1 - \xi\frac{K_{Lk}C_{PPIX}}{1 + K_{Lk}C_{PPIX}}\right)\times\left(C_{EtpI} - C_e \exp\left(\frac{2\Omega}{k_BT}\left(\gamma_0 - \frac{k_BTn_{k,0}}{a}\xi \ln(1 + K_{Lk}C_{PPIX})\right)\sqrt{\frac{K_{LS}C_{PPIX}}{S_0(1 + K_{LS}C_{PPIX})}}\right)\right) \quad (22)$$

where γ_0 is the surface free energy of the step edge in the absence of kink blockers.

The derived relation reflects the kink blocking activity of PPIX in the expression in the first parentheses. Step pinning, which modifies the step-solute equilibrium, is recognized by the exponential multiplier to C_e. The attenuation of the free energy of the step edge by PPIX interaction with the kinks is sanctioned by the parentheses-enclosed member in the argument of that exponential multiplier. Importantly, the relation in eq 22 emphasizes that the reduction of γ due to PPIX association to kinks denotes cooperativity between the step pinning and kink blocking modes of action of PPIX, as without step pinning, lower γ would not affect step growth. The diminished γ eases the passage of steps between the pinners and thus weakens the step pinning activity of PPIX, constituting an antagonistic element of the cooperativity between its two modes of action.

At constant C_{EtpI}, the rate law eq 22 predicts a sharp decline in v_R as PPIX is added to the solution, modeled by the expression in the first parentheses. In contrast to the

https://doi.org/10.1021/acs.cgd.1c00971
Cryst. Growth Des. 2021, 21, 7053−7064

straightforward kink blocking, however, eq 22 predicts complete growth cessation as soon as the modified C_{eR} reaches C_{EtpI}. If C_{PPIX} is fixed, the added activity of PPIX on the steps, to attenuate γ, weakens its step pinning capacity and shrinks the dead zone and the width of the transition from no growth to uninhibited step propagation in the $v(C_{EtpI})$ correlation. Notably, the (101), (111), and (001) faces of EtpI crystals do not cease to grow even at PPIX concentrations four-fold higher than what completely stunts step growth on the (010) face (Figure 4B,C). These faces are not accessible to AFM observations to deduce the relevant mechanisms of inhibition. We surmise that on these faces PPIX selects unique inhibition mechanisms that do not include step pinning, analogously to the anisotropic inhibition on the highly dissymmetric crystal surfaces of a potential nonopioid drug.[81]

How Do the Model Predictions Match the Experimental Data? The $v(C_{EtpI}, C_{PPIX})$ relation in eq 22 rests on four parameters: the top extent of kink inhibition ξ, the Langmuir constants for adsorption at the kinks K_{Lk} and on the crystal surface K_{LS}, and the surface free energy of the step edge in pure EtpI solutions γ_0. S-Shaped functions are defined by three parameters, and compliant experimental data may furnish their values. The functional dependence in eq 22, however, neglects the growth of straight step segments, and we expect it to poorly match the transition from stunted growth in the dead zone to uninhibited growth at high C_{EtpI}. Hence, fitting eq 22 to experimental results may at best yield two of the parameters that govern interactions of PPIX with kinks and surfaces. To fill in the missing two parameters, we estimate ξ and γ_0 from considerations unrelated to the $v(C_{EtpI}, C_{PPIX})$ data. Guided by previous determinations of ξ,[23] we assign it the value 0.5. We assume that at $C_{EtpI} - C_e > 0.2$ mM the steps are insensitive to PPIX adsorbed on the crystal surface, ascribe to the deceleration of v in this concentration range to kink blocking according to eq 5, and obtain $K_{Lk} = 1.1\ \mu M^{-1}$.

We relate γ_0 to the crystallization enthalpy ΔH^o_{cryst} via the Turnbull rule

$$\gamma_0 = \frac{0.3|\Delta H^o_{cryst}|}{N_A \Omega^{2/3}} \tag{23}$$

where N_A is Avogadro's number. Using $\Delta H^o_{cryst} = -26$ kJ mol^{-1} (ref 82) and $\Omega = 0.678$ nm^3 (ref 76) $\gamma_0 = 16$ mJ m^{-2}. This value of γ_0 coheres with $\gamma_0 = 23$ mJ m^{-2} for crystallization of hematin, another porphyrin, from a solvent dominated by octanol.[22,102,103] Applying the assumed ξ and the evaluated K_{Lk}, $-\Delta\gamma = 0.8$ mJ m^{-2} and $\gamma = 15$ mJ m^{-2}. Wielding the dead zone width $C_{eR} = 0.33$ mM (Figure 6A), its definition, eq 14, and the value of γ invokes $K_{LS} = 5 \times 10^{-3}\ \mu M^{-1}$. The ca. 200-fold discrepancy between K_{Lk} and K_{LS} is expected since a PPIX molecule invading a kink forms contacts with more molecules than it can with the relatively flat (010) surface of an EtpI crystal.

Incorporating the values of ξ, K_{Lk}, K_{LS}, and γ_0 in the relation for $v(C_{EtpI}, C_{PPIX})$, eq 22, reproduces relatively well the experimental data for $v(C_{PPIX})$ at constant C_{EtpI} (Figure 6B). The correspondence with the data for $v(C_{EtpI})$ at constant C_{PPIX}, however, is less precise, in particular, in the region of transition from the dead zone to fast step growth at high C_{EtpI} (Figure 6A). We accredit the inconsistency between the results of the model and the experimental quantities to the disparity between the modeled and measured step velocities. Equation 22 relates to the velocity of steps that curve to penetrate a fence of stoppers, whereas AFM measures velocities averaged over both curved and straight segments extant in the gaps between the stoppers.

Importantly, the $v(C_{EtpI}, C_{PPIX})$ rate law in eq 22 highlights the superiority of dual-action inhibitors as regulators of crystal growth. In contrast to modifiers that solely pin steps, dual-action inhibitors suppress step motion even at low concentrations (Figure 6B). They eclipse exclusive kink blockers as they invoke complete growth cessation if applied at elevated concentrations. At concentrations between these two extremes, dual-action inhibitors can dial in any degree of inhibition required to optimize the crystal size or shape.

Is Step Growth Suppression by Dual-Action Inhibitors Reversible? Deriving the relation in eq 22, we modeled the association of PPIX molecules to both kinks and flat crystal surfaces with the Langmuir adsorption law, an equilibrium expression that capitalizes on the assumption that adsorbed molecules readily desorb. A corollary of the adsorption reversibility is that if PPIX is removed from the solution, it would dissociate from the kinks and the crystal surface and allow step growth to return to its rate prior to PPIX introduction. The interaction of PPIX with kinks and surfaces, however, may elicit consequences excluded from the simplified model presented above. Among those are long-lasting lattice strain due to PPIX incorporation into the crystal[40,104] or the generation of defects that may both accelerate and depress crystal growth.[40,94,105,106] To test the reversibility of PPIX activity, we monitored how steps on the (010) face of the EtpI crystal evolve in response to the introduction and removal of PPIX from the solution (Figure 7).

In the presence of PPIX, the edge of the spiral step is serrated, which manifests the step pinning activity of the inhibitor (Figures 7A–C and 5B). The main characteristics of this shape persist, and the step velocity is relatively steady (Figure 7A–C,G). The introduction of solution of pure EtpI drastically remolds the growth spiral. The step edges straighten, and the characteristic lanceolate shape reemerges (Figure 7D–F). The rebuilt shape appears in the first AFM image, collected about 2 min after pure EtpI solution is pumped into the AFM cell, and it suggests that the desorption of PPIX from the surface has completed within this time. Surprisingly, the step velocity retains its reduced value for about 3 min after PPIX is purged. Steps that grow at ca. 8 nm s^{-1} (Figure 7G) and separate by about 1 μm (Figure 7D–F) contribute one or two layers to the crystal during this time. This estimate of the crystal matter that accumulates at a reduced rate after the removal of the inhibitor is consistent with a feasible mechanism of the transient irreversibility of step growth. We hypothesize that PPIX molecules that interact with the kinks and surfaces embed in the top crystal layers and strain them. The strain persists after PPIX is pulled out of the solution and continues to delay step growth until the accumulation of one or two crystal layers detaches the steps from the buried stress centers.

In about 3 min, step growth in solutions of pure EtpI recovers the rate driven by the employed C_{EtpI} (Figure 7G,H), and it implies that the observed irreversibility is constrained to short times after the inhibitor clears.

CONCLUSIONS

The example of etioporphyrin I crystals growing from solution in octanol in the presence of protoporphyrin IX reveals copious mechanistic details on crystallization control. We show

https://doi.org/10.1021/acs.cgd.1c00971
Cryst. Growth Des. 2021, 21, 7053–7064

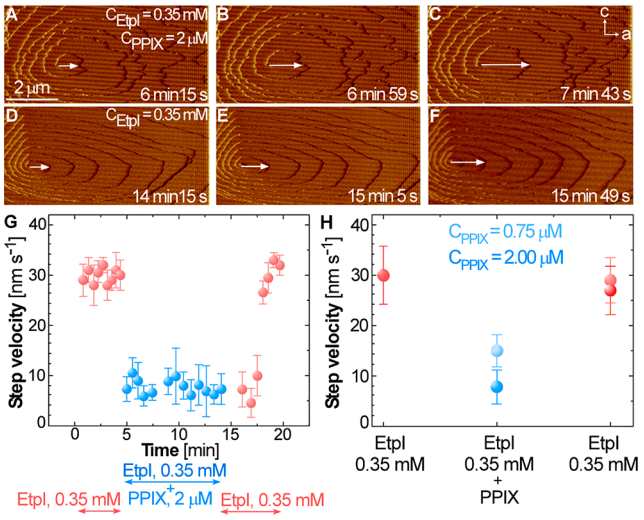

Figure 7. Transient responses of the spiral morphology and the step velocity to the introduction and removal of PPIX. (A–C) The configuration of a spiral step on the (010) face of EtpI crystals growing in a solution with C_{EtpI} = 0.35 mM in the presence of 2 μM PPIX. Indicated times start about 8 min after the PPIX-containing solution was introduced to the growth cell. (D–F) The evolution of the same spiral step as in A–C in a solution of EtpI only with C_{EtpI} = 0.35 mM. Indicated times start about 2 min after the solution in A–C was replaced with a solution of EtpI only. (G) The evolution of the step velocity in the [100] direction in a solution with C_{EtpI} = 0.35 mM, after this solution was replaced with a solution of both EtpI and PPIX with C_{EtpI} = 0.35 mM and C_{PPIX} = 2 μM at 5 min, and after the initial solution of pure EtpI replaced the solution of EtpI and PPIX at 15 min. (H) The average velocities of steps in solutions of pure EtpI with C_{EtpI} = 0.35 mM, after PPIX was added, at 0.75 μM, and, in a separate experiment, at 2 μM, and after the PPIX-containing solutions were replaced with a pure EtpI solution with C_{EtpI} = 0.35 mM. Light blue and red and dark blue and red symbols denote results of two distinct experiments.

that despite the hugely divergent structures of kinks and surfaces an inhibitor may bind to both interface elements and exert a dual mode of crystallization suppression. We demonstrate that dual-action inhibitors are superior regulators of crystal growth that afford the opportunity to fine-tune the degree of inhibitions required to optimize the growth and shape of a crystal of interest. The activity of PPIX is constrained to blocking kinks and pinning steps and excludes aftereffects that may permanently delay step motion, such as strain in the crystal lattice. We show that the reduction of the step edge free energy, a necessary condition for association to kinks and blocking the solute access to them, attenuates the step pinning activity of the inhibitor. We put forth a closed-form rate law for step growth in the presence of a dual-action modifier that highlights an antagonistic element of the cooperativity of the activity modes enforced by the decline of step edge free energy.

It is tempting to ascribe the dual action of PPIX to its structural similarity to the solute, EtpI. A higher level of understanding of how a modifier molecule associates to a kink or a flat crystal surface that may come from DFT and all-atom MD simulations may assess the significance of similarity between solute and modifier and help to design better dual-action inhibitors.

None of the mechanisms recruited by PPIX to inhibit the growth of EtpI crystals appear unique to organic crystallization. Limiting the interactions between solute, solvent, and modifier exclusively to van der Waals forces may direct the governing parameters of these mechanisms, but the results that we present stop short of elucidating the underlying pathways.

Numerous additional questions remain open. Among them are whether a modifier that employs a certain mode of action on one crystal face would similarly inhibit the other faces in the crystal habit. The common use of step pinners in the crystallization practice demands that an analytical model that adequately captures the variable relative contributions of straight and curved steps moving among a field of stoppers is soon developed so that crystal growth can be predictably and accurately tailored by inhibitors. On a grander scale, the rational selection of modifiers to control the synthesis of crystals of interest seems like a blue-sky goal, but it may succumb to an integrated effort that combines the predictions of advanced models with data obtained in carefully staged experiments.

■ ASSOCIATED CONTENT

Supporting Information

The Supporting Information is available free of charge at https://pubs.acs.org/doi/10.1021/acs.cgd.1c00971.

Materials and methods, Figure S1, Table S1 (PDF)

■ AUTHOR INFORMATION

Corresponding Author

Peter G. Vekilov − *Department of Chemical and Biomolecular Engineering, University of Houston, Houston, Texas 77204-4004, United States; Department of Chemistry, University of Houston, Houston, Texas 77204-5003, United States;* orcid.org/0000-0002-3424-8720; Email: vekilov@uh.edu

Author

Rajshree Chakrabarti − *Department of Chemical and Biomolecular Engineering, University of Houston, Houston, Texas 77204-4004, United States*

Complete contact information is available at: https://pubs.acs.org/10.1021/acs.cgd.1c00971

Funding

This work was supported by the National Science Foundation (Award No. DMR-2128121) and NIH (Award No. R01 AI150763).

Notes

The authors declare no competing financial interest.

■ ACKNOWLEDGMENTS

We thank Monika Warzecha for helpful discussions and suggestions and for X-ray identification of the EtpI crystal faces, Sima MafiMoghaddam for help with the graphics, and James F. Lutsko for insightful suggestions on the dual-action model development.

■ REFERENCES

(1) Dodson, G.; Steiner, D. The role of assembly in insulin's biosynthesis. *Curr. Opin. Struct. Biol.* **1998**, *8*, 189–194.

(2) Georgiou, D. K.; Vekilov, P. G. A fast response mechanism for insulin storage in crystals may involve kink generation by association of 2D clusters. *Proc. Natl. Acad. Sci. U. S. A.* **2006**, *103*, 1681–1686.

(3) Hirsch, R. E.; Lin, M. J.; Nagel, R. L. The inhibition of hemoglobin C crystallization by hemoglobin F. *J. Biol. Chem.* **1988**, *263*, 5936−9.
(4) Canterino, J. E.; Galkin, O.; Vekilov, P. G.; Hirsch, R. E. Phase Separation and Crystallization of Hemoglobin C in Transgenic Mouse and Human Erythrocytes. *Biophys. J.* **2008**, *95*, 4025−4033.
(5) Plomp, M.; Carroll, A. M.; Setlow, P.; Malkin, A. J. Architecture and assembly of the Bacillus subtilis spore coat. *PLoS One* **2014**, *9*, e108560.
(6) Weiner, S.; Addadi, L. Design strategies in mineralized biological materials. *J. Mater. Chem.* **1997**, *7*, 689−702.
(7) Weiner, S.; Dove, P. M. An overview of biomineralization processes and the problem of the vital effect. *Biomineralization* **2003**, *54*, 1−29.
(8) Davis, K. J.; Dove, P. M.; De Yoreo, J. J. The role of Mg2+ as an impurity in calcite growth. *Science* **2000**, *290*, 1134−1137.
(9) Myerson, A. S. *Handbook of Industrial Crystallization*, 3rd ed.; Cambridge University Press: Cambridge, 2019.
(10) De Yoreo, J. J.; Burnham, A. K.; Whitman, P. K. Developing KH_2PO_4 and KD_2PO_4 crystals for the world's most powerful laser. *Int. Mater. Rev.* **2002**, *47*, 113−152.
(11) Orme, C. A.; Noy, A.; Wierzbicki, A.; McBride, M. T.; Grantham, M.; Teng, H. H.; Dove, P. M.; DeYoreo, J. J. Formation of chiral morphologies through selective binding of amino acids to calcite surface steps. *Nature* **2001**, *411*, 775−779.
(12) Teng, H. H.; Dove, P. M.; Orme, C. A.; De Yoreo, J. J. Thermodynamics of Calcite Growth: Baseline for Understanding Biomineral Formation. *Science* **1998**, *282*, 724.
(13) Rimer, J. D.; An, Z.; Zhu, Z.; Lee, M. H.; Goldfarb, D. S.; Wesson, J. A.; Ward, M. D. Crystal growth inhibitors for the prevention of L-cystine kidney stones through molecular design. *Science (Washington, DC, U. S.)* **2010**, *330*, 337−341.
(14) Reznikov, N.; Steele, J. A. M.; Fratzl, P.; Stevens, M. M. A materials science vision of extracellular matrix mineralization. *Nature Reviews Materials* **2016**, *1*, 16041.
(15) Song, X.; Yang, X.; Zhang, T.; Zhang, H.; Zhang, Q.; Hu, D.; Chang, X.; Li, Y.; Chen, Z.; Jia, M.; Zhang, P.; Yu, J. Controlling the Morphology and Titanium Coordination States of TS-1 Zeolites by Crystal Growth Modifier. *Inorg. Chem.* **2020**, *59*, 13201−13210.
(16) Sanhoob, M. A.; Muraza, O.; Al-Mutairi, E. M.; Ullah, N. Role of crystal growth modifiers in the synthesis of ZSM-12 zeolite. *Adv. Powder Technol.* **2015**, *26*, 188−192.
(17) Lupulescu, A. I.; Kumar, M.; Rimer, J. D. A Facile Strategy To Design Zeolite L Crystals with Tunable Morphology and Surface Architecture. *J. Am. Chem. Soc.* **2013**, *135*, 6608−6617.
(18) Liang, Y.; Jacobson, A. J.; Rimer, J. D. Strontium Ions Function as Both an Accelerant and Structure-Directing Agent of Chabazite Crystallization. *ACS Materials Letters* **2021**, *3*, 187−192.
(19) Olafson, K. N.; Li, R.; Alamani, B. G.; Rimer, J. D. Engineering Crystal Modifiers: Bridging Classical and Nonclassical Crystallization. *Chem. Mater.* **2016**, *28*, 8453−8465.
(20) Chung, J.; Granja, I.; Taylor, M. G.; Mpourmpakis, G.; Asplin, J. R.; Rimer, J. D. Molecular modifiers reveal a mechanism of pathological crystal growth inhibition. *Nature* **2016**, *536*, 446−450.
(21) Basavaraj, D. R.; Biyani, C. S.; Browning, A. J.; Cartledge, J. J. The Role of Urinary Kidney Stone Inhibitors and Promoters in the Pathogenesis of Calcium Containing Renal Stones. *EAU-EBU Update Series* **2007**, *5*, 126−136.
(22) Olafson, K. N.; Ketchum, M. A.; Rimer, J. D.; Vekilov, P. G. Mechanisms of hematin crystallization and inhibition by the antimalarial drug chloroquine. *Proc. Natl. Acad. Sci. U. S. A.* **2015**, *112*, 4946−4951.
(23) Ma, W.; Lutsko, J. F.; Rimer, J. D.; Vekilov, P. G. Antagonistic cooperativity between crystal growth modifiers. *Nature* **2020**, *577*, 497−501.
(24) Nakai, K.; Tazuma, S.; Nishioka, T.; Chayama, K. Inhibition of cholesterol crystallization under bilirubin deconjugation: partial characterization of mechanisms whereby infected bile accelerates pigment stone formation. *Biochim. Biophys. Acta, Mol. Cell Biol. Lipids* **2003**, *1632*, 48−54.
(25) Kibe, A.; Holzbach, R. T.; LaRusso, N. F.; Mao, S. J. Inhibition of cholesterol crystal formation by apolipoproteins in supersaturated model bile. *Science* **1984**, *225*, 514.
(26) Busch, N.; Matiuck, N.; Sahlin, S.; Pillay, S. P.; Holzbach, R. T. Inhibition and promotion of cholesterol crystallization by protein fractions from normal human gallbladder bile. *J. Lipid Res.* **1991**, *32*, 695−702.
(27) de Villiers, K. A.; Egan, T. J. Heme Detoxification in the Malaria Parasite: A Target for Antimalarial Drug Development. *Acc. Chem. Res.* **2021**, *54*, 2649.
(28) Kapishnikov, S.; Hempelmann, E.; Elbaum, M.; Als-Nielsen, J.; Leiserowitz, L. Malaria Pigment Crystals: The Achilles' Heel of the Malaria Parasite. *ChemMedChem* **2021**, *16*, 1515−1532.
(29) Sullivan, D. J. Quinolines block every step of malaria heme crystal growth. *Proc. Natl. Acad. Sci. U. S. A.* **2017**, *114*, 7483−7485.
(30) Sullivan, D. J.; Gluzman, I. Y.; Russell, D. G.; Goldberg, D. E. On the molecular mechanism of chloroquine's antimalarial action. *Proc. Natl. Acad. Sci. U. S. A.* **1996**, *93*, 11865−11870.
(31) Sullivan, D. J.; Matile, H.; Ridley, R. G.; Goldberg, D. E. A Common Mechanism for Blockade of Heme Polymerization by Antimalarial Quinolines. *J. Biol. Chem.* **1998**, *273*, 31103−31107.
(32) Rimer, J. D.; An, Z.; Zhu, Z.; Lee, M. H.; Goldfarb, D. S.; Wesson, J. A.; Ward, M. D. Crystal growth inhibitors for the prevention of L-cystine kidney stones through molecular design. *Science* **2010**, *330*, 337−41.
(33) Olafson, K. N.; Nguyen, T. Q.; Rimer, J. D.; Vekilov, P. G. Antimalarials inhibit hematin crystallization by unique drug−surface site interactions. *Proc. Natl. Acad. Sci. U. S. A.* **2017**, *114*, 7531−7536.
(34) Olafson, K. N.; Nguyen, T. Q.; Vekilov, P. G.; Rimer, J. D. Deconstructing Quinoline-Class Antimalarials to Identify Fundamental Physicochemical Properties of Beta-Hematin Crystal Growth Inhibitors. *Chem. - Eur. J.* **2017**, *23*, 13638−13647.
(35) Chung, J.; Granja, I.; Taylor, M. G.; Mpourmpakis, G.; Asplin, J. R.; Rimer, J. D. Molecular modifiers reveal a mechanism of pathological crystal growth inhibition. *Nature* **2016**, *536*, 446−450.
(36) Stranski, I. N. Zur Theorie des Kristallwachstums. *Z. Phys. Chem.* **1928**, *136U*, 259−278.
(37) Kaischew, R. Zur Theorie des Kristallwaschstums. *Eur. Phys. J. A* **1936**, *102*, 684−690.
(38) Burton, W. K.; Cabrera, N.; Frank, F. C. The growth of crystals and equilibrium structure of their surfaces. *Philos. Trans. R. Soc. London Ser. A* **1951**, *243*, 299−360.
(39) Chernov, A. A. The spiral growth of crystals. *Sov. Phys. Uspekhi* **1961**, *4*, 116−148.
(40) Chernov, A. A. *Modern Crystallography III, Crystal Growth*; Springer: Berlin, 1984.
(41) Lovette, M. A.; Browning, A. R.; Griffin, D. W.; Sizemore, J. P.; Snyder, R. C.; Doherty, M. F. Crystal Shape Engineering. *Ind. Eng. Chem. Res.* **2008**, *47*, 9812−9833.
(42) Gorka, A. P.; de Dios, A.; Roepe, P. D. Quinoline Drug−Heme Interactions and Implications for Antimalarial Cytostatic versus Cytocidal Activities. *J. Med. Chem.* **2013**, *56*, 5231−5246.
(43) Yau, S.-T.; Thomas, B. R.; Galkin, O.; Gliko, O.; Vekilov, P. G. Molecular mechanisms of microheterogeneity-induced defect formation in ferritin crystallization. *Proteins: Struct., Funct., Genet.* **2001**, *43*, 343−352.
(44) Cabrera, N.; Vermilyea, D. A. The growth of crystals form solution. In *Growth and Perfection of Crystals*, Doremus, R. H.; Roberts, B. W.; Turnbul, D., Eds.; Wiley: New York, 1958; Vol. *393−408*.
(45) Potapenko, S. Y. Threshold for step percolation through impurity fence. *J. Cryst. Growth* **1993**, *133*, 141−146.
(46) Potapenko, S. Y. Moving of step through impurity fence. *J. Cryst. Growth* **1993**, *133*, 147−154.
(47) Wang, L.; Zhang, W.; Qiu, S. R.; Zachowicz, W. J.; Guan, X.; Tang, R.; Hoyer, J. R.; Yoreo, J. J. D.; Nancollas, G. H. Inhibition of

https://doi.org/10.1021/acs.cgd.1c00971
Cryst. Growth Des. 2021, 21, 7053−7064

calcium oxalate monohydrate crystallization by the combination of citrate and osteopontin. *J. Cryst. Growth* **2006**, *291*, 160−165.
(48) Weaver, M. L.; Qiu, S. R.; Hoyer, J. R.; Casey, W. H.; Nancollas, G. H.; De Yoreo, J. J. Improved model for inhibition of pathological mineralization based on citrate−calcium oxalate monohydrate interaction. *ChemPhysChem* **2006**, *7*, 2081−2084.
(49) Weaver, M. L.; Qiu, S. R.; Hoyer, J. R.; Casey, W. H.; Nancollas, G. H.; De Yoreo, J. J. Inhibition of calcium oxalate monohydrate growth by citrate and the effect of the background electrolyte. *J. Cryst. Growth* **2007**, *306*, 135−145.
(50) De Yoreo, J. J.; Wang, W.; Tsukamoto, K.; Wu, D. Physical Mechanisms of Crystal Growth Modification by Biomolecules. *AIP Conf. Proc.* **2010**, *1270*, 45−58.
(51) Lutsko, J. F.; González-Segredo, N.; Durán-Olivencia, M. A.; Maes, D.; Van Driessche, A. E. S.; Sleutel, M. Crystal Growth Cessation Revisited: The Physical Basis of Step Pinning. *Cryst. Growth Des.* **2014**, *14*, 6129−6134.
(52) Voronkov, V. V.; Rashkovich, L. N. Influence of mobile adsorbed impurity on the motion of steps. *Sov. Phys. Crystallogr.* **1992**, *37*, 289−295.
(53) Voronkov, V. V.; Rashkovich, L. N. Step kinetics in the presence of mobile adsorbed impurity. *J. Cryst. Growth* **1994**, *144*, 107−115.
(54) Chernov, A. A.; Rashkovich, L. N.; Mkrtchan, A. A. Solution growth kinetics and mechanism: primatic face of KDP. *J. Cryst. Growth* **1986**, *74*, 101−112.
(55) Chernov, A. A.; Rashkovich, L. N.; Smol'sky, I. L.; Kuznetsov, Y. G.; Mkrtchan, A. A.; Malkin, A. I. Processes of growth of crystals from aqueous solutions. In *Growth of Crystals*; Givargizov, E. E., Ed.; Consultant Bureau: New York, 1986; Vol. *15*, pp 43−91.
(56) Shtukenberg, A. G.; Ward, M. D.; Kahr, B. Crystal growth with macromolecular additives. *Chem. Rev.* **2017**, *117*, 14042−14090.
(57) Land, T. A.; Martin, T. L.; Potapenko, S.; Palmore, G. T.; De Yoreo, J. J. Recovery of surfaces from impurity poisoning during crystal growth. *Nature* **1999**, *399*, 442−445.
(58) Davis, K. J.; Dove, P. M.; De Yoreo, J. J. The Role of Mg^{2+} as an Impurity in Calcite Growth. *Science* **2000**, *290*, 1134−1137.
(59) Poloni, L. N.; Zhu, Z.; Garcia-Vázquez, N.; Yu, A. C.; Connors, D. M.; Hu, L.; Sahota, A.; Ward, M. D.; Shtukenberg, A. G. Role of Molecular Recognition in l-Cystine Crystal Growth Inhibition. *Cryst. Growth Des.* **2017**, *17*, 2767−2781.
(60) Vekilov, P. G. Nonclassical Nucleation. In *Crystallization via Nonclassical Pathways Vol. 1: Nucleation, Assembly, Observation & Application*; American Chemical Society, 2020; Vol. *1358*, pp 19−46.
(61) Warzecha, M.; Florence, A. J.; Vekilov, P. G. The ambiguous functions of the precursors that enable nonclassical modes of olanzapine nucleation and growth. *Crystals* **2021**, *11*, 738.
(62) De Yoreo, J. A Perspective on Multistep Pathways of Nucleation. In *Crystallization via Nonclassical Pathways Vol. 1: Nucleation, Assembly, Observation & Application*; American Chemical Society, 2020; Vol. *1358*, pp 1−17.
(63) De Yoreo, J. J.; Gilbert, P. U. P. A.; Sommerdijk, N. A. J. M.; Penn, R. L.; Whitelam, S.; Joester, D.; Zhang, H.; Rimer, J. D.; Navrotsky, A.; Banfield, J. F.; Wallace, A. F.; Michel, F. M.; Meldrum, F. C.; Cölfen, H.; Dove, P. M. Crystallization by particle attachment in synthetic, biogenic, and geologic environments. *Science* **2015**, *349*, aaa6760.
(64) Warzecha, M.; Verma, L.; Johnston, B. F.; Palmer, J. C.; Florence, A. J.; Vekilov, P. G. Olanzapine crystal symmetry originates in preformed centrosymmetric solute dimers. *Nat. Chem.* **2020**, *12*, 914−920.
(65) Lupulescu, A. I.; Rimer, J. D. In Situ Imaging of Silicalite-1 Surface Growth Reveals the Mechanism of Crystallization. *Science* **2014**, *344*, 729−732.
(66) Kumar, M.; Luo, H.; Román-Leshkov, Y.; Rimer, J. D. SSZ-13 Crystallization by Particle Attachment and Deterministic Pathways to Crystal Size Control. *J. Am. Chem. Soc.* **2015**, *137*, 13007−13017.
(67) Gliko, O.; Neumaier, N.; Pan, W.; Haase, I.; Fischer, M.; Bacher, A.; Weinkauf, S.; Vekilov, P. G. A metastable prerequisite for the growth of lumazine synthase crystals. *J. Am. Chem. Soc.* **2005**, *127*, 3433−3438.
(68) Gliko, O.; Pan, W.; Katsonis, P.; Neumaier, N.; Galkin, O.; Weinkauf, S.; Vekilov, P. G. Metastable liquid clusters in super- and undersaturated protein solutions. *J. Phys. Chem. B* **2007**, *111*, 3106−3114.
(69) Ma, W.; Balta, V. A.; West, R.; Newlin, K. N.; Miljanić, O. Š.; Sullivan, D. J.; Vekilov, P. G.; Rimer, J. D. A second mechanism employed by artemisinins to suppress Plasmodium falciparum hinges on inhibition of hematin crystallization. *J. Biol. Chem.* **2021**, *296*, 100123.
(70) Qin, W.; Agarwal, A.; Choudhary, M. K.; Palmer, J. C.; Rimer, J. D. Molecular Modifiers Suppress Nonclassical Pathways of Zeolite Crystallization. *Chem. Mater.* **2019**, *31*, 3228−3238.
(71) Lupulescu, A. I.; Qin, W.; Rimer, J. D. Tuning Zeolite Precursor Interactions by Switching the Valence of Polyamine Modifiers. *Langmuir* **2016**, *32*, 11888.
(72) Rae Cho, K.; Kim, Y.-Y.; Yang, P.; Cai, W.; Pan, H.; Kulak, A. N.; Lau, J. L.; Kulshreshtha, P.; Armes, S. P.; Meldrum, F. C.; De Yoreo, J. J. Direct observation of mineral−organic composite formation reveals occlusion mechanism. *Nat. Commun.* **2016**, *7*, 10187.
(73) Meldrum, F. C.; Cölfen, H. Controlling Mineral Morphologies and Structures in Biological and Synthetic Systems. *Chem. Rev.* **2008**, *108*, 4332−4432.
(74) Farmanesh, S.; Ramamoorthy, S.; Chung, J.; Asplin, J. R.; Karande, P.; Rimer, J. D. Specificity of Growth Inhibitors and their Cooperative Effects in Calcium Oxalate Monohydrate Crystallization. *J. Am. Chem. Soc.* **2014**, *136*, 367−376.
(75) Sangwal, K. *Additives and Crystallization Processes: From Fundamentals to Applications*; John Wiley & Sons, 2007.
(76) Che, C.-M.; Xiang, H.-F.; Chui, S. S.-Y.; Xu, Z.-X.; Roy, V. A. L.; Yan, J. J.; Fu, W.-F.; Lai, P. T.; Williams, I. D. A High-Performance Organic Field-Effect Transistor Based on Platinum(II) Porphyrin: Peripheral Substituents on Porphyrin Ligand Significantly Affect Film Structure and Charge Mobility. *Chem. - Asian J.* **2008**, *3*, 1092−1103.
(77) Hoang, M. H.; Kim, Y.; Kim, M.; Kim, K. H.; Lee, T. W.; Nguyen, D. N.; Kim, S.-J.; Lee, K.; Lee, S. J.; Choi, D. H. Unusually High-Performing Organic Field-Effect Transistors Based on π-Extended Semiconducting Porphyrins. *Adv. Mater.* **2012**, *24*, 5363−5367.
(78) Hoang, M. H.; Kim, Y.; Kim, S.-J.; Choi, D. H.; Lee, S. J. High-Performance Single-Crystal-Based Organic Field-Effect Transistors from π-Extended Porphyrin Derivatives. *Chem. - Eur. J.* **2011**, *17*, 7772−7776.
(79) Lahav, M.; Leiserowitz, L. Tailor-made auxiliaries for the control of nucleation, growth and dissolution of two- and three-dimensional crystals. *J. Phys. D: Appl. Phys.* **1993**, *26*, B22−B31.
(80) Kahr, B.; Shtukenberg, A. G.; Yang, J.; Ward, M. D. Tailor-Made Auxiliaries for Polar Growth from Melts. *Isr. J. Chem.* **2021**, *61*, 583−589.
(81) Poloni, L. N.; Ford, A. P.; Ward, M. D. Site Discrimination and Anisotropic Growth Inhibition by Molecular Imposters on Highly Dissymmetric Crystal Surfaces. *Cryst. Growth Des.* **2016**, *16*, 5525−5541.
(82) Chakrabarti, R. G.; Vekilov, P. G. Attraction between Permanent Dipoles and London Dispersion Forces Dominate the Thermodynamics of Organic Crystallization. *Cryst. Growth Des.* **2020**, *20*, 7429−7438.
(83) Dandekar, P.; Kuvadia, Z. B.; Doherty, M. F. Engineering Crystal Morphology. *Annu. Rev. Mater. Res.* **2013**, *43*, 359−386.
(84) Macrae, C. F.; Sovago, I.; Cottrell, S. J.; Galek, P. T. A.; McCabe, P.; Pidcock, E.; Platings, M.; Shields, G. P.; Stevens, J. S.; Towler, M.; Wood, P. A. Mercury 4.0: from visualization to analysis, design and prediction. *J. Appl. Crystallogr.* **2020**, *53*, 226−235.
(85) Dam, B.; Bennema, P.; Van Enckevort, W. J. P. The mechanism of tapering on KDP-type crystals. *J. Cryst. Growth* **1986**, *74*, 118−128.

https://doi.org/10.1021/acs.cgd.1c00971
Cryst. Growth Des. 2021, 21, 7053−7064

(86) Giovannetti, R. The Use of Spectrophotometry UV-Vis for the Study of Porphyrins. In *Macro To Nano Spectroscopy*; Uddin, J., Ed.; IntechOpen: Rijeka, 2012.
(87) Bruhn, T.; Brückner, C. The origin of the absorption spectra of porphyrin N- and dithiaporphyrin S-oxides in their neutral and protonated states. *Phys. Chem. Chem. Phys.* **2015**, *17*, 3560−3569.
(88) Kano, K.; Minamizono, H.; Kitae, T.; Negi, S. Self-Aggregation of Cationic Porphyrins in Water. Can $\pi-\pi$ Stacking Interaction Overcome Electrostatic Repulsive Force? *J. Phys. Chem. A* **1997**, *101*, 6118−6124.
(89) Dvornikov, S. S.; Solov'ev, K. N.; Tsvirko, M. P. Spectroscopic manifestations of dimerization of etioporphyrin I in hydrocarbon solvents. *J. Appl. Spectrosc.* **1983**, *38*, 581−585.
(90) PaineIII, J. B., III; Dolphin, D.; Gouterman, M. Exciton and electron interaction in covalently-linked dimeric porphyrins. *Can. J. Chem.* **1978**, *56*, 1712−1715.
(91) Vekilov, P. G.; Kuznetsov, Y. G.; Chernov, A. A. Interstep interaction in solution growth; (101) ADP face. *J. Cryst. Growth* **1992**, *121*, 643−655.
(92) Vekilov, P. G.; Kuznetsov, Y. G.; Chernov, A. A. The effect of temperature on step motion; (101) ADP face. *J. Cryst. Growth* **1992**, *121*, 44−52.
(93) Kossel, W. *Nachr. Ges. Wiss. Götingen* **1928**, 135−138.
(94) Yau, S.-T.; Thomas, B. R.; Vekilov, P. G. Molecular mechanisms of crystallization and defect formation. *Phys. Rev. Lett.* **2000**, *85*, 353−356.
(95) Gibbs, J. W. On the equilibrium of heterogeneous substances, First Part. *Trans. Connect. Acad. Sci.* **1876**, *3*, 108−248.
(96) Eyring, H.; Lin, S. H.; Lin, S. M. *Basic Chemical Kinetics*; John Wiley and Sons: New York, 1980.
(97) De Yoreo, J. J.; Vekilov, P. G. Principles of crystal nucleation and growth. *Biomineralization* **2003**, *54*, 57−93.
(98) Rashkovich, L. N. *KDP-Family Single Crystals*; Adam Hilger: Bristol, 1991.
(99) Kubota, N.; Mullin, J. W. A kinetic model for crystal growth from aqueous solution in the presence of impurity. *J. Cryst. Growth* **1995**, *152*, 203−208.
(100) Lee-Thorp, J. P.; Shtukenberg, A. G.; Kohn, R. V. Effect of Step Anisotropy on Crystal Growth Inhibition by Immobile Impurity Stoppers. *Cryst. Growth Des.* **2017**, *17*, 5474−5487.
(101) von Szyszkowski, B. Experimentelle Studien über kapillare Eigenschaften der wässerigen Lösungen von Fettsäuren. *Z. Phys. Chem.* **1908**, *64*, 385−414.
(102) Olafson, K. N.; Ketchum, M. A.; Rimer, J. D.; Vekilov, P. G. Molecular Mechanisms of Hematin Crystallization from Organic Solvent. *Cryst. Growth Des.* **2015**, *15*, 5535−5542.
(103) Olafson, K. N.; Rimer, J. D.; Vekilov, P. G. Early Onset of Kinetic Roughening due to a Finite Step Width in Hematin Crystallization. *Phys. Rev. Lett.* **2017**, *119*, 198101.
(104) Vekilov, P. G.; Monaco, L. A.; Thomas, B. R.; Stojanoff, V.; Rosenberger, F. Repartitioning of NaCl and protein impurities in lysozyme crystallization. *Acta Crystallogr., Sect. D: Biol. Crystallogr.* **1996**, *52*, 785−798.
(105) Chernov, A. A.; Smol'skii, I. L.; Parvov, V. F.; Kuznetsov, Y. G.; Rozhanskii, V. N. X-ray diffraction investigation of the growth of ADP crystals. *Sov. Phys. Crystallogr.* **1980**, *25*, 469−474.
(106) Yau, S.-T.; Petsev, D. N.; Thomas, B. R.; Vekilov, P. G. Molecular-level thermodynamic and kinetic parameters for the self-assembly of apoferritin molecules into crystals. *J. Mol. Biol.* **2000**, *303*, 667−678.

https://doi.org/10.1021/acs.cgd.1c00971
Cryst. Growth Des. 2021, 21, 7053−7064